3D Thermo-Acoustic Modeling of a Piezoelectric Transducer for Directed Interstitial Ultrasound Ablation

K. Y. Gandomi[1], Z. Zhao[1], M. Tarasek[2], E. W. Fiveland[2], C. Bhushan[2], G. Ghoshal[3], P. Neubauer[3], E. Williams[3], M. Liu[1], P. A. Carvalho[1], C. J. Nycz[1], D. Yeo[2], E. C. Burdette[3], and G. S. Fischer [1]

[1]Worcester Polytechnic Institute, Worcester, MA, USA
[2]General Electric Global Research, Niskayuna, NY, USA
[3]Acoustic Medsystems Inc, Savoy, IL, USA

Abstract

Thermal ablation is a treatment option in oncology that can be used to target primary and metastatic cancers. In this approach, high temperature heating is administered at the target tumor site to induce coagulative necrosis of malignant cells. One minimally invasive method for administering thermal ablation is interstitial needle-based therapeutic ultrasound (NBTU). The NBTU approach delivers a cylindrical piezoelectric transducer that produces high frequency ultrasound waves at the target tumor location, leading to localized heating and death of cancer cells. In this work, we present a three-dimensional (3D) model of an existing 90° directional piezoelectric transducer currently used by an NBTU applicator in pre-clinical studies and provide a preliminary validation of the simulation using magnetic resonance thermal imaging (MRTI).

Introduction

Cancer is a healthcare concern worldwide, with a projected 1,762,450 new cases in the United States in 2019 [1]. Treatment options are determined by the physician based on the clinical case and they may choose to apply immunotherapy, chemotherapy, thermotherapy, or surgical intervention. Thermal ablation is one such treatment option in oncology for targeting primary and metastatic cancers unsuited for traditional surgical interventions. The use of high temperature applicators to deliver heating or ablation, to induce localized malignant cell death, has been previously studied [2,3]. The required heat deposition can be administered using microwaves [4], radiofrequency [5], lasers [6], and intra- [7] or extra- [8] corporeal ultrasound.

One minimally invasive method for administering thermal ablation is interstitial needle-based therapeutic ultrasound (NBTU). The NBTU applicator is used to deliver a piezoelectric transducer to the target tumor location. When the transducer is electrically excited, high intensity acoustic waves are produced and absorbed by the cancerous cells, leading to localized heating and cell death. The use of a piezoelectric material by the NBTU approach offers good spatial control over the produced beam pattern as the geometry of the transducer can be manipulated to achieve a desired beam shape and directionality. Applicator designs with sectored cylindrical [9], planar [10], and multi-element [11] transducers have been demonstrated in literature.

Numerical modeling of the acoustic pressure field produced by the deforming piezoelectric transducer is often performed to characterize the energy deposition of the NBTU applicator and optimize the element design for thermal dose delivery during treatment. The resulting pressure field is then provided as input to the bioheat transfer equation to observe the thermal propagation by the applicator over time. Experimental validation of these results can be performed using magnetic resonance thermal imaging (MRTI). This is often computed using the proton resonant frequency shift (PRFS) method to calculate quantitative spatial temperature maps from phase differences in the magnetic field [12, 13]. Material specific parameter calibration can also be performed to improve these temperature measurements during tissue heating [14].

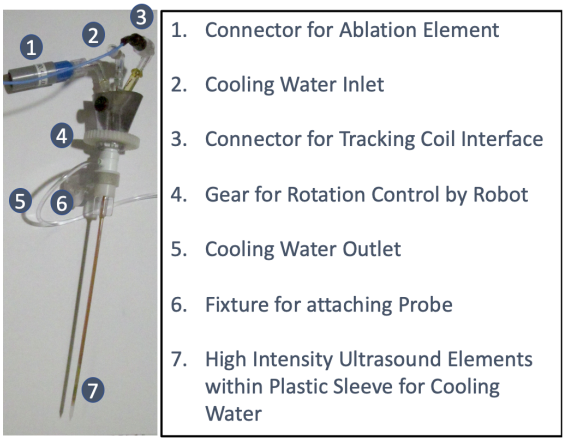

Figure 1. MRI Compatible NBTU probe with labeled components simulated in this paper and developed by Acoustic Medsystems Inc for interstitial thermal ablation.

In this work, we present a three-dimensional (3D) model of an existing 90° directional piezoelectric transducer currently used by an NBTU applicator in preclinical studies. We extend our previously developed two-dimensional model [15] and discuss the steps taken to move to a three dimensional model. An eigenmode analysis, frequency domain study, and bioheat transfer time

domain study are presented. The results demonstrate the outcome for our NBTU applicator, but can be extended to other transducer geometries to inform studies focused on NBTU applicator design for cancer intervention. We also present an initial validation of our model by comparing the results with our physical NBTU applicator activated under MR-thermometry.

Operating Principle

The principles used to develop ultrasound transducers have been well studied in prior art [16, 17]. These devices are often constructed using piezoelectric materials that strain when subjected to an applied electric potential. There are a variety of naturally occurring substances that can produce this inverse piezoelectric effect such as quartz and lithium niobate. However, ferroceramics such as lead zirconium titanate (PZT) are commonly used for their wide bandwith. In particular, for thermal therapy applications, PZT-4 is often selected for it's low loss properties.

Each transducer operates at an ideal driving excitation frequency (resonance) to produce ultrasonic waves through a desired acoustic medium. The geometry of the transducer can be modified to produce a desired ultrasonic beam pattern as demonstrated by cylindrical, sectored cylindrical, and planar element designs. The applied electric potential to the transducer drives the deformation and contributes to the overall energy deposition of the generated waves.

The medium that the transducer operates within has a key impact on the transmission of the produced ultrasonic wave and determines beam properties such as absorption and attenuation. For heat deposition, the ultrasound intensity within the region of interest along with the medium thermal conductivity and heat capacity will dictate the spatial thermal pattern and propagation induced by the transducer. Often, there are ineffeciencies of the transducer to convert mechanical energy into acoustic energy that result in self-heating. To compensate for this effect, water can be circulated through the length of the transducer housing as demonstrated in [18] to limit thermal contributions external to the generated ultrasound waves. In this work, however, thermal conduction from this circulating water was not modeled.

Simulation Setup

The physical NBTU probe developed by Acoustic Medsystems Inc (Illinois, United States) and modeled in the presented COMSOL 5.5 simulation is shown in figure 1. A three dimensional (3D) COMSOL component was created using the built in geometry tools to create a 1.5mm outer diameter by 1.1mm inner diameter by 5mm tall cylinder. Four notches of 0.1mm depth by 0.05mm width were also added such that the probe was segmented into 90° and 180° sectors. Lead zirconate titanate (PZT-4) from the COMSOL material library was selected as the probe cylinder material with no modifications and simulation properties for the transducer are shown in table 1.

The solid mechanics physics interface defined the transducer as a piezoelectric material and defined a fixed constraint within the inner surface of the cylinder. The piezoelectric poling direction was defined by a base vector coordinate system defined by the transform shown in table 2 and was aligned radially outward from the center of the transducer geometry. The electrostatics physics interface was also used to define a 14V electric potential along the 90° outer surface of the transducer and to define a ground constraint along the inner surface.

Table 1. Simulation properties of the modeled NBTU applicator

NBTU Properties	
Ceramic Material	PZT-4
Density	7500 (kg/m^3)
Resonant Frequency	5.0444 MHz
Electric Potential	14V

Table 2. Base vector coordinate frame used to give the poling direction of the piezoelectric element.

Base Vectors	x	y	z
x1	-sin(atan2(Y,X))	cos(atan2(Y,X))	0
x2	0	0	1
x3	cos(atan2(Y,X))	sin(atan2(Y,X))	0

Table 3. Material Properties of the Simulated Acoustic Medium

Acoustic Medium Properties	
Heat Capacity	3451 (J/(kg*K))
Density	1058 (kg/m^3)
Thermal Conductivity	0.53 (W/(m*K))
Speed of Sound	1151 (m/s)
Attenuation	31.96 Np/m

The medium surrounding the transducer cylinder is composed of a 10mm by 4mm by 6mm (LxWxH) homogeneous block. Outside the block there is a 0.5mm thick perfectly matched layer (PML) that covers the entire tissue area to absorb the outgoing waves and minimize signal reflection. The working area of the simulation was then defined as a quarter of the acoustic medium to leverage the up-down and left-right symmetry in the acoustic field as observed in our previous 2D simulations [15] and to simplify 3D study calculations. This quarter region is illustrated on the transducer in figure 2 along with a display of other simulation properties. This simplified geometry setup with the transducer and acoustic medium are shown

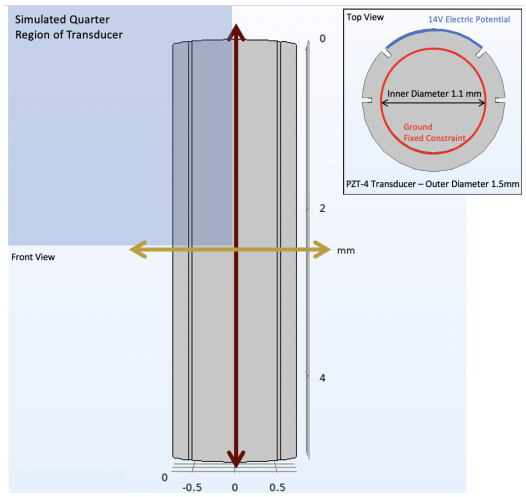

Figure 2. Front and top view schematic of the transducer geometry with simulation parameters and properties displayed. A quarter region of the transducer is also shown and simulated to simplify 3D volume calculations based on produced beam symmetry observed in our previous works.

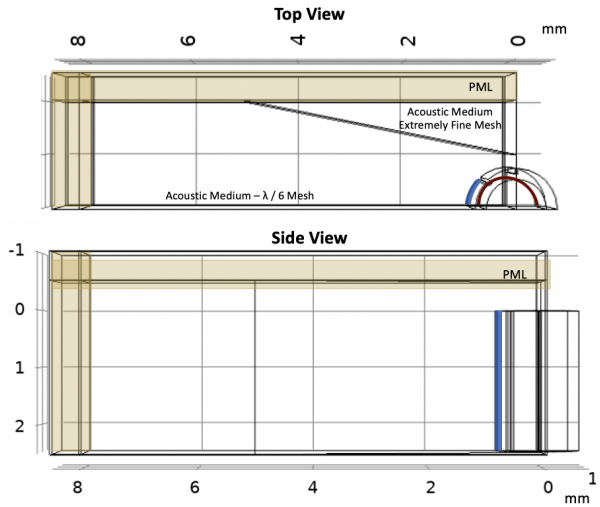

Figure 3. COMSOL 5.5 3D probe geometry setup using quarter segment of the acoustic field. Blue surface represents the 90° sector that has an applied electric potential in the simulations.

in figure 3. The medium was given custom material properties shown in table 3 based on the measured results from the acoustic phantom recipe presented in Farrer et al. [19]

The pressure acoustics physics interface was used to define the wave propagation through the medium as a linear elastic fluid model with an attenuation coefficient of 31.96 Np/m. The bioheat transfer physics interface was used to defined a heat source applied to the medium with a user defined activation function shown in equation 1, where Q is the absorbed ultrasound energy over the acoustic field, $acpr.Q_{pw}$ is the dissipated power intensity, $step$ is a COMSOL step function from 0 to 1 with smoothing of 0.005, t is the current time step of the simulation, and $t_{probeOn}$ is a constant that represents the total time the transducer should be activated. Dynamic tissue properties such as blood perfusion were not considered in this version of the simulation, but should be accounted for to more accurately represent heating within the desired anatomy.

$$Q = acpr.Q_{pw} * step(t - t_{probeOn}) \quad (1)$$

3D Meshing and Cluster Computing

From previous work, we knew that the wave propagation pattern was directional and created a 90° ultrasonic beam pattern that attenuated with distance from the source [15]. The quarter region representing the acoustic medium was separated into two sections to simplify the model and to control the mesh resolution in the region of interest. The first section was the region of beam propagation and required a high resolution tetrahedral mesh with a maximum element size of $\lambda/6$, where λ represents the wavelength of the emitted acoustic beam, in order to accurately view the produced ultrasonic waves. The second section represents all other regions within the acoustic medium outside of the main beam pattern. Here, a lower resolution extremely fine mesh was used with a maximum element size of 0.925mm. The location of these two mesh sections is shown in the simulation setup in figure 3. The PML region was meshed using the "swept" feature to create a five layer structured prism mesh. A "Boundary Layer Mesh" consisting of a single mesh layer with a thickness of $\lambda/12$ was also created between the inner free-tetrahedral meshes and the surrounding structured PML mesh in order to create a smooth transition between the two regions and yield a more precise far-field calculation.

The studies for this 3D transducer simulation required large volume computations that can benefit from leveraging increased resources and task distribution of cluster computing. This approach has significant benefits in the case of limited computing resources of a typical single desktop computer, i.e. not enough memory or CPU power for large models. In this work, a Linux based cluster was used to compute the simulations using COMSOL 5.5 in batches. Instead of processing the model as a whole, COMSOL can distribute small sections and process them on multiple compute nodes simultaneously using Microsoft Message Passing Interface (MPI). The Turing research cluster (Linux based with a SLURM® job scheduler) at Worcester Polytechnic Institute (WPI) was used to submit multi-node batch jobs using shell scripts for computing the presented 3D simulation. Four computer nodes each equipped with two Intel® Xeon® Platinum 8168 CPU at 2.70 GHz with 12 cores and 150GB of memory per node were allocated as resources to compute the studies in this simulation. The acoustic pressure field

frequency domain study in particular was the largest calculation performed using the 3D transducer model and required solving for 9,359,860 degrees of freedom. The computation time using the cluster was 7h14min8s, which is 5 hours shorter when compared to a single workstation (2 x Intel® Xeon® Gold 6148 CPU at 2.40GHz with 40 cores in total and 384GB memory) that computed the same simulation in 12h9min48s. The use of the cluster can be more efficient and less time consuming than running the same simulation on the GUI version of COMSOL.

Resonant Frequency and Eigenmode Analysis

Piezoelectric transducers have natural resonant frequencies that are determined by the geometry, poling, and material of the element. To determine these key frequencies for the transducer, a COMSOL boundary probe was placed on the 90° surface of the transducer to measure total displacement, *solid.disp*. A frequency domain study was used to sweep from 1 MHz to 10 MHz at 0.1 kHz steps to find those frequencies that induce the highest transducer deformation. The result of this sweep is shown in figure 4 with the greatest deformation at 5.0444 MHz. The 3D deformation produced by the transducer at this frequency can also be evaluated using an eigenmode study and is also shown in figure 4.

Acoustic Pressure Field Frequency Domain Study

The generated ultrasound waves produced by the transducer can be simulated in COMSOL using a frequency domain study at the selected resonant mode. The frequency domain study uses the pressure acoustics, solid mechanics, and electrostatics physics interfaces. The resulting acoustic pressure field is shown in figure 5 and depicts a 90° high intensity ultrasonic beam pattern that attenuates with distance from the source. Wave interference in the produced beam can also be observed as shown within the black square in figure 6. The produced wave propagation induced by the probe surface deformation is controlled by the eigenmode analysis and meshing configurations which may contribute to this effect. Lower intensity side lobes from the transducer edges are also perceptible and shown within the red square in figure 6.

Bioheat Transfer Time Domain Study

The heat produced by the deposited ultrasound energy into the medium can be modeled in COMSOL using a time domain study using the acoustic pressure field calculated in the previous section. This study used the bioheat transfer physics interface and simulated a 60 second ablation with a 60 second cool down period at 1 second time steps. The resulting temperature field at the peak of the insonation period is shown in figure 7 and depicts a 90° directional heating pattern when viewed from the top.

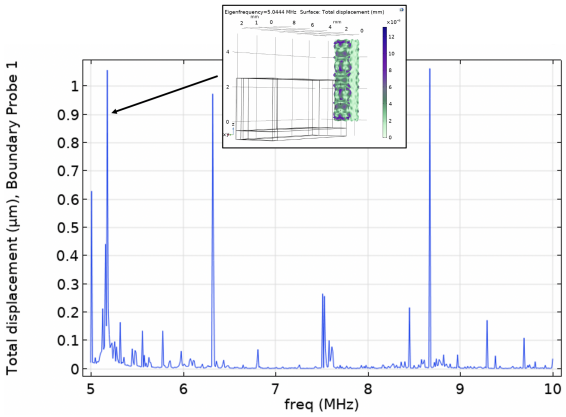

Figure 4. Frequency sweep from 5MHz to 10MHz at 0.1 kHz steps that is used to show the location of greatest deformation by the transducer and the deformation of the element at this location.

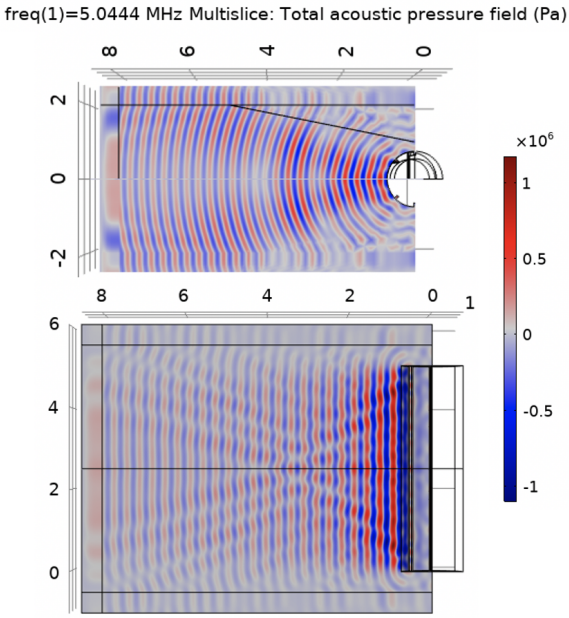

Figure 5. Top and side view of the simulated acoustic pressure field for the 3D applicator with a 90° beam pattern.

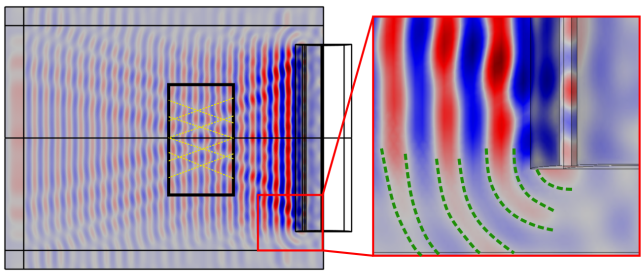

Figure 6. Side view of the acoustic pressure field showing wave interference within the black square and low intensity acoustic fringing at the transducer edges in the zoomed-in red square.

From the side view, thermal propagation along the edges of the transducer is also visible.

MR-Thermometry of Physical Applicator

An experimental validation of the developed three-dimensional (3D) model was performed using a physical needle based therapeutic ultrasound (NBTU) probe activated under magnetic resonance thermal imaging (MRTI). The probe was inserted approximately 30mm within an 100mm by 100mm by 250mm (LxWxH) homogeneous porcine skin gelatin phantom as shown in figure 8. The phantom was built using the recipe from Farrer et al. [19] and approximates the material properties used by the simulated acoustic medium. The probe-phantom setup was placed within a GE head coil and centered in the bore of a 3T GE Signa Architect scanner (GE Healthcare, Waukesha, WI).

A single-echo spoiled gradient echo (SPGR) imaging sequence was taken of the probe-phantom setup to calculate referenced phase difference maps for corrected PRFS MR-thermometry. The sequence parameters included echo time (TE) = 13.2ms, repetition time (TR) = 93ms, flip angle (θ) = 30°, field of view (FoV) = (15x15)cm^2, matrix size = (256x256), 7 slice acquisition, and slice thickness = 2mm. The PRFS maps were corrected by the interpolated phase difference maps of the non-heated outer edge region of the phantom [20]. The PRFS thermal coefficient was assumed to be that of water-based tissues with a value of -0.01 $ppm/^oC$. The NBTU probe was then turned ON using the Theravision software (Acoustic Medsystems Inc, Illinois, United States). The ablation was conducted for 60 seconds and then the probe was turned OFF and allowed to cool back to room temperature (20°). The experiment was repeated for two perpendicular scan plan orientations.

The resulting temperature maps from the collected MR data is compared with the simulated bioheat transfer results in figures 9 and 10 after 60 seconds of ablation. A vertical line of temperature readings crossing through $z = 0$ and $X = 0$ are plotted against position in figure 9(c) and 10(c) for the top and side view results respectively. An RMS error between the simulated and experimental line plots was computed and yielded a 1.56^oC error for the side view and 1.87^oC error for the top view. These preliminary results suggest good agreement, however, a more in depth calibration of simulation parameters and comparison with the experimental data should be conducted to fully validate the model across all time steps.

Conclusion

A simulation for a three-dimensional (3D) piezoelectric transducer with a 90° directional ablation pattern is presented. The model was built based on the design of an existing needle based therapeutic ultrasound (NBTU) probe

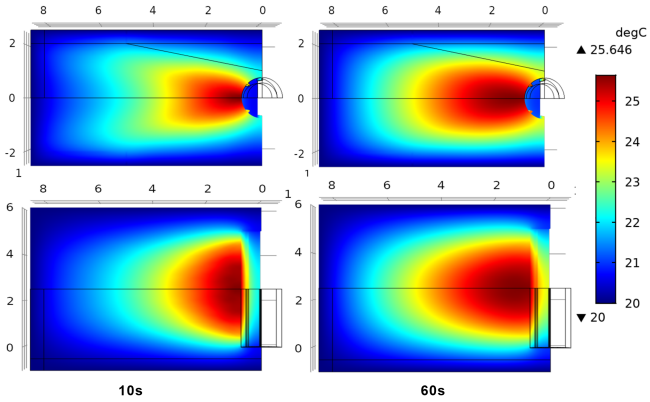

Figure 7. Top and side view of the simulated bioheat transfer for the 3D applicator at 10s and 60s of ablation.

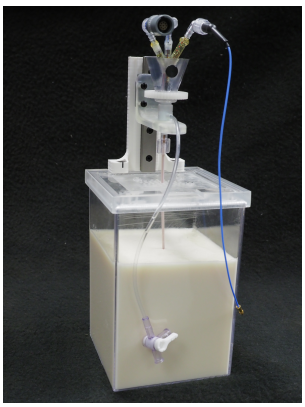

Figure 8. Experimental setup of physical NBTU applicator within a homogeneous porcine skin gelatin phantom of known acoustic properties for MR-validation.

used in pre-clinical thermal ablation studies. In this work, an eigenmode analysis demonstrates the deformation by the probe at the piezoelectric level. A frequency domain study with a sufficiently fine mesh resolution was created by leveraging symmetry in the model and shows the produced high intensity ultrasound waves emitted by the transducer. A bioheat transfer time domain study was then computed for the model and compared with temperature maps from the physical applicator collected under MR-thermometry. Future work will focus on improving the calibration between the model and the experimental results, creating a 3D simulation of a rotating transducer similar to the 2D version presented in [21], and investigation of non-static material properties such as blood perfusion to more accurately represent heating within the desired anatomy.

Funding Data

- National Institutes of Health (NIH) under the National Cancer Insitutiton (NCI) (Grant No. R01 CA166379)

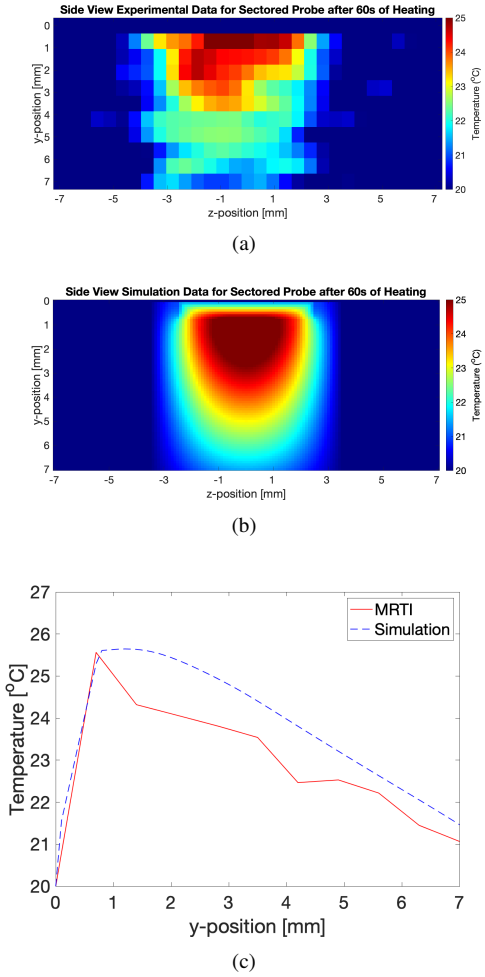

Figure 9. Side view of (a) the experimental MRTI data and (b) the simulated bioheat transfer results after 60 seconds of ablation. Temperature values through the middle of the temperature maps at z=0 are plotted in (c) for comparison.

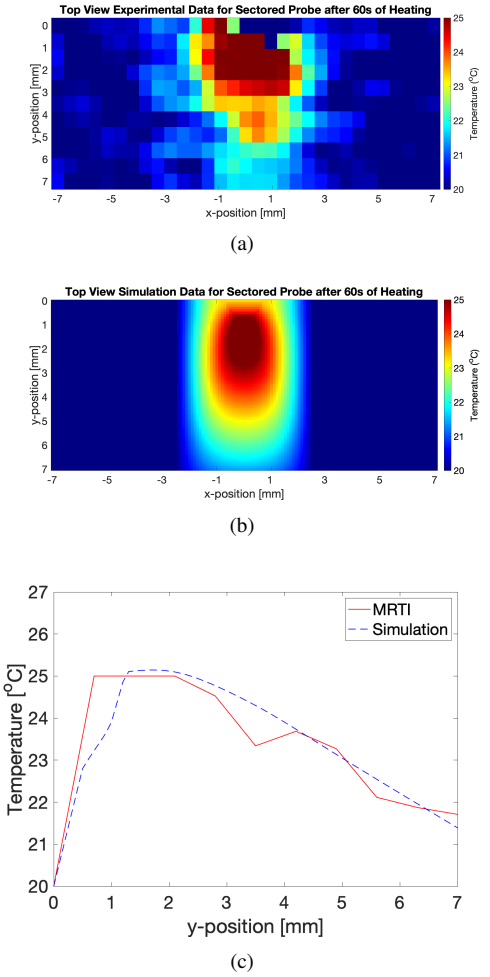

Figure 10. Top view of (a) the experimental MRTI data and (b) the simulated bioheat transfer results after 60 seconds of ablation. Temperature values through the middle of the temperature maps at x=0 are plotted in (c) for comparison.

References

1. Siegel, R. L., Miller, K. D. & Jemal, A. Cancer statistics, 2019. *CA: A Cancer J. for Clin.* **69**, 7–34, DOI: 10.3322/caac.21551. https://acsjournals.onlinelibrary.wiley.com/doi/pdf/10.3322/caac.21551.

2. Diederich, C. J. Thermal ablation and high-temperature thermal therapy: Overview of technology and clinical implementation. *Int. J. Hyperth.* **21**, 745–753, DOI: 10.1080/02656730500271692 (2005). https://doi.org/10.1080/02656730500271692.

3. Haemmerich, D. & Laeseke, P. F. Thermal tumour ablation: Devices, clinical applications and future directions. *Int. J. Hyperth.* **21**, 755–760, DOI: 10.1080/02656730500226423 (2005). https://doi.org/10.1080/02656730500226423.

4. Carrafiello, G. *et al.* Microwave tumors ablation: Principles, clinical applications and review of preliminary experiences. *Int. J. Surg.* **6**, S65 – S69, DOI: https://doi.org/10.1016/j.ijsu.2008.12.028 (2008).

5. Ni, Y., Mulier, S., Miao, Y., Michel, L. & Marchal, G. A review of the general aspects of radiofrequency ablation. *Abdom. imaging* **30**, 381–400 (2005).

6. Stafford, R. J., Fuentes, D., Elliott, A. A., Weinberg, J. S. & Ahrar, K. Laser-induced thermal therapy for tumor ablation. *Critical Rev. Biomed. Eng.* **38** (2010).

7. Lafon, C., Melodelima, D., Salomir, R. & Chapelon, J. Y. Interstitial devices for minimally invasive thermal ablation by high-intensity ultrasound. *Int. J. Hyperth.* **23**, 153–163, DOI: 10.1080/

02656730601173029 (2007). https://doi.org/10.1080/02656730601173029.

8. ter Haar, D. G. & Coussios, C. High intensity focused ultrasound: Physical principles and devices. *Int. J. Hyperth.* **23**, 89–104, DOI: 10.1080/02656730601186138 (2007). PMID: 17578335, https://doi.org/10.1080/02656730601186138.

9. Diederich, C. J. *et al.* Transurethral ultrasound applicators with directional heating patterns for prostate thermal therapy: In vivo evaluation using magnetic resonance thermometry. *Med. Phys.* **31**, 405–413, DOI: 10.1118/1.1639959 (2004). https://aapm.onlinelibrary.wiley.com/doi/pdf/10.1118/1.1639959.

10. Chopra, R., Luginbuhl, C., Weymouth, A. J., Foster, F. S. & Bronskill, M. J. *Phys. Medicine Biol.* **46**, 3133–3145, DOI: 10.1088/0031-9155/46/12/305 (2001).

11. Melodelima, D., Lafon, C., Prat, F., Birer, A. & Cathignol, D. Ultrasound cylindrical phased array for transoesophageal thermal therapy: initial studies. *Phys. Medicine Biol.* **47**, 4191–4203, DOI: 10.1088/0031-9155/47/23/306 (2002).

12. Ishihara, Y. *et al.* A precise and fast temperature mapping using water proton chemical shift. *Magn. Reson. Medicine* **34**, 814–823, DOI: 10.1002/mrm.1910340606 (1995). https://onlinelibrary.wiley.com/doi/pdf/10.1002/mrm.1910340606.

13. Poorter, J. D. *et al.* Noninvasive mri thermometry with the proton resonance frequency (prf) method: In vivo results in human muscle. *Magn. Reson. Medicine* **33**, 74–81, DOI: 10.1002/mrm.1910330111 (1995). https://onlinelibrary.wiley.com/doi/pdf/10.1002/mrm.1910330111.

14. Tarasek, M. R. *et al.* Validation of mr thermometry: Method for temperature probe sensor registration accuracy in head and neck phantoms. *Int. J. Hyperth.* **30**, 142–149, DOI: 10.3109/02656736.2014.887794 (2014). https://doi.org/10.3109/02656736.2014.887794.

15. Gandomi, K. *et al.* Thermo-acoustic simulation of a piezoelectric transducer for interstitial thermal ablation with mrti based validation. .

16. Jaffe, H. & Berlincourt, D. Piezoelectric transducer materials. *Proc. IEEE* **53**, 1372–1386 (1965).

17. Fry, W. J., Mosberg, W., Barnard, J. & Fry, F. Production of focal destructive lesions in the central nervous system with ultrasound. *J. neurosurgery* **11**, 471–478 (1954).

18. Diederich, C. *et al.* Catheter-based ultrasound applicators for selective thermal ablation: progress towards mri-guided applications in prostate. *Int. journal hyperthermia* **20**, 739–756 (2004).

19. Farrer, A. I. *et al.* Characterization and evaluation of tissue-mimicking gelatin phantoms for use with mrgfus. *J. therapeutic ultrasound* **3**, 9 (2015).

20. Shmatukha, A. V., Harvey, P. R. & Bakker, C. J. Correction of proton resonance frequency shift temperature maps for magnetic field disturbances using fat signal. *J. Magn. Reson. Imaging* **25**, 579–587, DOI: 10.1002/jmri.20835 (2007). https://onlinelibrary.wiley.com/doi/pdf/10.1002/jmri.20835.

21. Gandomi, K. *et al.* Modeling of interstitial ultrasound ablation for continuous applicator rotation with mr validation. *IEEE Transactions on Biomed. Eng.* 1–1 (2020).